Research Article

Cancer Immunology Research

Coexpression of Inhibitory Receptors Enriches for Activated and Functional CD8$^+$ T Cells in Murine Syngeneic Tumor Models

Huizhong Xiong[1], Stephanie Mittman[1], Ryan Rodriguez[1], Patricia Pacheco-Sanchez[1], Marina Moskalenko[1], Yagai Yang[1], Justin Elstrott[2], Alex T. Ritter[3], Sören Müller[4], Dorothee Nickles[4], Teresita L. Arenzana[3], Aude-Hélène Capietto[3], Lélia Delamarre[3], Zora Modrusan[5], Sascha Rutz[3], Ira Mellman[3], and Rafael Cubas[1]

Abstract

Exhausted T cells have been described in cancer patients and murine tumor models largely based on their expression of various inhibitory receptors. Understanding of the functional attributes of these cells is limited. Here, we report that among CD8$^+$ T cells in commonly used syngeneic tumor models, the coexpression of inhibitory receptors PD-1, LAG3, and TIM3 defined a group of highly activated and functional effector cells. Coexpression of these receptors further enriched for antigen-specific cells with increased T-cell receptor clonality. Anti–PD-L1 treatment increased the number and activation of these triple-positive CD8$^+$ T cells without affecting the density of PD-1$^-$ cells. The intratumoral density of CD8$^+$ T cells coexpressing inhibitory receptors negatively correlated with tumor burden. The density ratio and pretreatment phenotype of CD8$^+$ T cells coexpressing inhibitory receptors was positively correlated with response across a variety of tumor models. Our results demonstrate that coexpression of inhibitory receptors is not a signifier of exhausted T cells, but rather can define a group of activated and functional effector cells in syngeneic tumor models. In the cancer setting, these cells could represent a heterogeneous population of not only exhausted but also highly activated cells responsive to treatment.

Introduction

T cells help eliminate infections and malignant cells. When infections or tumors are not completely eliminated, T cells become persistently exposed to antigen, which can cause a state of dysfunction known as exhaustion, characterized by altered phenotypic and transcriptional profiles (1–3). Most definitions for exhausted T cells (Tex) come from chronic viral infection models (2–7), where progressive development of Tex cells is associated with the coexpression of inhibitory receptors such as programmed death-1 (PD-1), lymphocyte-activation gene 3 (LAG3), and T-cell immunoglobulin and mucin-domain containing-3 (TIM3), a hierarchical loss of effector functions, and an altered transcriptional program and chromatin state partly involving a shift in the balance between T-bet and EOMES (1, 5, 6, 8–11).

PD-1$^+$ T cells are frequently observed in cancer patients. Especially when PD-1 expression is accompanied by other inhibitory receptors, these cells are presumed to represent Tex cells whose reinvigoration by blocking the interaction between PD-1 and its ligand PD-L1 underlies the clinical success of anti–PD-1/PD-L1 therapies (12–17). Evidence from chronic lymphocytic choriomeningitis virus (LCMV) infection suggests that early-stage T-bet^{hi}PD-1^{int} Tex cells can be reinvigorated by anti–PD-L1 treatment driving improved functional output that partially overlaps with effector T cells. Terminal stage EOMES^{hi} Tex cells coexpress PD-1, LAG3, and TIM3, lose their effector functions and do not respond to anti–PD-1/PD-L1 treatment (12). A stem-like CD8$^+$ T-cell population expressing PD-1, CXCR5, and the transcription factor TCF1 may undergo a proliferative burst following PD-1 blockade (18).

Studies suggest that PD-1/LAG3/TIM3 expressing CD8$^+$ T cells are exhausted and dysfunctional (5, 6, 9, 19), and that targeting LAG3 or TIM3 together with anti–PD-1/PD-L1 is a viable strategy to reinforce antitumor responses (5, 9, 19, 20). However, understanding of the development, function, and heterogeneity of Tex cells in the cancer setting and whether these cells are the main responders to checkpoint blockade remains incomplete.

Although inhibitory receptors such as PD-1, LAG3, and TIM3 are used to define Tex cells, these molecules are also upregulated following activation and effector cell differentiation (21–23), calling into question the validity of their use to define Tex cells. PD-1$^+$LAG3$^+$TIM3$^+$ CD8$^+$ T cells are heterogeneous (2, 10, 11, 18), and LAG3 and TIM3 expression may actually be associated with cytotoxic T lymphocyte (CTL) function. An enrichment of PD-1$^+$ CD8$^+$ T cells coexpressing LAG3 and/or TIM3 within tumor antigen–specific T-cell repertoires with high antitumoral

[1]Department of Translational Oncology, Genentech, South San Francisco, California. [2]Department of Biomedical Imaging, Genentech, South San Francisco, California. [3]Department of Cancer Immunology, Genentech, South San Francisco, California. [4]Department of Bioinformatics and Computational Biology, Genentech, South San Francisco, California. [5]Department of Molecular Biology, Genentech, South San Francisco, California.

Note: Supplementary data for this article are available at Cancer Immunology Research Online (http://cancerimmunolres.aacrjournals.org/).

Corresponding Author: Rafael Cubas, Genentech, 1 DNA Way MS-50, South San Francisco, CA, 94080. Phone: 650-225-1539; E-mail: cubasr@gene.com

Cancer Immunol Res 2019;7:963–76

doi: 10.1158/2326-6066.CIR-18-0750

activity has been observed in melanoma patients and tumor-bearing animals (24, 25). Additionally, enhanced PD-1, LAG3, and TIM3 expression was found on tissue-resident memory-like $CD8^+$ tumor-infiltrating lymphocytes (TIL), which expressed IFNγ and granzyme B (GZMB), and was associated with better survival outcome in lung cancer patients and murine tumor models (26, 27). In another study using single-cell profiling, high PD-1 and TIM3 expression was uncoupled from dysfunction and, instead, was clustered with costimulatory receptors, indicating shared regulatory mechanisms (28). Even in the chronic LCMV model, PD-1^+TIM3^+ $CD8^+$ T cells highly expressed granzymes and perforin, but showed lower TNFα and IL2 expression, suggestive of a more terminal effector differentiated state (18).

Although inhibitory receptor expression is largely associated with T_{ex} cells, these markers can also define highly activated cells in the cancer setting. Understanding the heterogeneity of $CD8^+$ T cells coexpressing inhibitory receptors will be instrumental in defining the mechanism of action of checkpoint inhibitor therapies. Here, we investigated the phenotype of intratumoral $CD8^+$ T cells in commonly used syngeneic tumor models and their response to anti–PD-L1 treatment. Our data demonstrate that, far from being exhausted, these cells display an activated phenotype with cytotoxic and effector potential. Their numbers and activation state are augmented following anti–PD-L1 treatment. Additionally, the number of $CD8^+$ T cells coexpressing inhibitory receptors negatively correlated with tumor burden and the density ratio and pretreatment phenotype of these cells correlated with response across a variety of responsive and nonresponsive tumor models.

Materials and Methods

Animal study oversight

All animal studies were reviewed and approved by Genentech's Institutional Animal Care and Use Committee. Mice whose tumors exceeded acceptable size limits (2,000 mm^3) or became ulcerated were euthanized and removed from the study.

Mice

Eight- to 10-week-old female C57Bl/6 or Balb/C mice were obtained from The Charles River Laboratories and housed at Genentech in standard rodent micro-isolator cages to be acclimated to study conditions for at least 3 days before tumor cell implantation.

Antibodies

For animal studies, murine IgG1 anti–PD-L1 clone 6E11 and murine IgG1 anti-gp120 isotype control antibody were used. Antibodies were stored in 20 mmol/L histidine acetate, 240 mmol/L sucrose, and 0.02% polysorbate 20, pH 5.5 and diluted in PBS prior to use. For flow cytometry analysis, the following fluorochrome-conjugated mAbs to the following mouse proteins were used: CD45 (clone 30-F11, 1:100), TIM3 (clone RMT3-23, 1:100), ICOS (clone C398.4A, 1:100), CD25 (clone PC61, 1:100), OX40 (clone OX-86, 1:100), and T-bet (clone 4B10, 1:20) were purchased from BioLegend. MAbs to mouse CD4 (clone RM4-5, 1:100), CD8 (clone 53-6.7, 1:100), PD1 (clone 29F.1A12, 1:100), PD-L1 (clone 10F.9G2, 1:200), and LAG3 (clone C9B7W, 1:100) were all from BD Biosciences. mAbs to mouse EOMES (clone Dan11mag, 1:80), TNFα (clone MP6-XT22, 1:100), IFNγ (clone MP6-XT22, 1:100), CD69 (clone H1.2F3, 1:100), Ki67 (clone SolA15, 1:100), CD62L (clone Mel14, 1:80), and CD44 (clones IM7, 1:200) were from eBioscience. Anti-human granzyme B (cross-reacts with mouse; clone MHGB05, 1:100) was purchased from Life Technologies. LIVE/DEAD Fixable Dead Cell Stain from Life Technologies was used to gate on live cells.

For intracellular staining, the following reagents were used: eBioscience Foxp3 Fix/Perm buffer kit (Thermo Fisher), Cell Stimulation Cocktail (Thermo Fisher), and GolgiStop (Thermo Fisher).

Cell lines

The murine colon adenocarcinoma MC38 cell line was obtained from a former Genentech colleague, Rink Offringa, in 2008. Murine mammary carcinoma EMT6, JC, and 4T1 cell lines were obtained from ATCC (2016, 2008, and 2006, respectively), tested for *Mycoplasma* using the MycoAlert Mycoplasma Detection Kit (Lonza), kept at low passage numbers and maintained in complete RPMI-1640 medium (HyClone) supplemented with 10% heat-inactivated premium grade FBS (VWR) and 2.05 mmol/L L-glutamine. These cell lines were not authenticated in the past year.

Cells were cultured in RPMI-1640 medium plus 2 mmol/L L-glutamine with 10% fetal bovine serum (HyClone). Cells in log-phase growth were centrifuged, washed once with Hank's balanced salt solution (HBSS), counted, and resuspended in 50% HBSS and 50% Matrigel (BD Biosciences) at 1×10^6 cells/mL for injection into mice.

Syngeneic tumor studies

Tumor cells were harvested in log-phase growth and resuspended in HBSS containing Matrigel (BD Biosciences) at a 1:1 ratio. For MC38, tumor cells were implanted subcutaneously in the right unilateral thoracic area of C57Bl/6 mice at 0.1 million MC38 cells. For EMT6, JC, and 4T1, Balb/C mice were inoculated in the left mammary fat pad #5 with 0.1 million cells. Tumors were monitored until they became established and reached a mean tumor volume of ~190 mm^3. Mice with tumors in the range of 130–250 mm^3 were then randomized into treatment groups. Treatment was initiated the next day with either isotype control antibody (gp120 mIgG1) or anti–PD-L1 mIgG1 (clone 6E11) at 10 mg/kg intravenously (i.v.) for the first dose followed by 5 mg/kg intraperitoneally (i.p.) thereafter twice a week up to 3 weeks (for efficacy studies).

Tumor volumes and body weights were measured twice per week. Tumor volumes were measured in two dimensions (length and width) using Ultra Cal-IV calipers (Fred V. Fowler Co.) and volume was calculated using the formula: Tumor size (mm^3) = (length × $width^2$) × 0.5. Mice body weights were measured using an Adventurer Pro AV812 scale (Ohaus Corporation). Antibodies were diluted in histidine buffer (20 mmol/L histidine acetate, 240 mmol/L sucrose, and 0.02% polysorbate 20, pH 5.5).

Flow cytometry

To generate single-cell suspensions, tumors were collected, cut into 2–4 mm pieces, and digested for 30 minutes using the murine Tumor Dissociation Kit from Miltenyi (Miltenyi Biotec) following the manufacturer's instructions (cat. 130-096-730). Tumor homogenates were filtered through a 70-μm nylon filter (Corning) and washed twice with RPMI-1640 media. After the last wash, cells were resuspended in staining buffer (PBS + 0.5% FCS + 5 mmol/L EDTA). Cells were surface-stained for 25 minutes at

4°C. For intracellular staining, cells were fixed and permeabilized using the eBioscience Foxp3 Fix/Perm buffer kit. For detection of IFNγ and TNFα, cells were stimulated with Cell Stimulation Cocktail for 5 hours. After 1 hour, GolgiStop was added to the cells. FACS analyses were performed using a Symphony flow cytometer (BD Biosciences). Data were analyzed using FlowJo software (Tree Star, Inc.).

Tetramer staining and peptide stimulation

Tumor lysates were stained with PE and PE-CF594-conjugated peptide–MHCI tetramers for 20 minutes at room temperature followed by staining with cell-surface and intracellular markers. Tetramers specific for the following sequences were pooled at a final concentration of 20 μg/mL each for each fluorophore:

Reps1: AQLANDVVL
Adpgk: ASMTNMELM
P15e: KSPWFTTL
M86: KILTFDRL

For peptide stimulation, tumor lysates were incubated with complete medium containing 10 μg/mL of peptides (pooled) and 5 μg/mL of IL2 for 6 hours in the presence of BD GolgiPlug before proceeding to surface and intracellular staining. See also Yadav and colleagues (29). The peptide sequences used were as follows:

Reps1: GRVLELFRAAQLANDVVLQIMELC
Adpgk: IPVHLELASMTNMELMSSIVHQQV
P15e: QGWFEGLFNKSPWFTTLISTIM
M86: ILKAGGKILTFDRLALESPKGRGT

***In vitro* calcium flux assay**

Murine P815 tumor cells were genetically modified using the PiggyBac transposon system (Systems Biosciences) to overexpress the genetically encoded calcium indicator GCaMP6s (30) and full-length human HER2. The cell line was generated from a single-cell clone to ensure a tight expression range of hHER2 and GCaMP6s proteins. Murine T cells and tumor cells were stained with Celltrace yellow and Celltrace far red dyes (Thermo), respectively, to provide a stable signal for image segmentation and analysis. For imaging, cells were cultured in phenol red-free RPMI (GIBGO) with 2% FBS. Tumor cells were plated on the surface of an 8-well glass imaging chamber (Cellvis) coated with recombinant murine ICAM-I (R&D Systems). T cells were then added and allowed to settle onto the surface of the glass. The T-cell/tumor cell coculture was imaged for 5 minutes prior to the addition of a bispecific antibody consisting of anti-HER2 (4D5) and anti-muCD3e(2C11; ref. 29). T-cell/target interaction was imaged using a Ti3 inverted widefield microscope (Nikon) with a brick and block stage incubation system (Nikon Instruments) at 37°C, 5% CO_2 under 200× magnification.

T cells and tumor cells were analyzed using the Spots and Surfaces functions, respectively, in Imaris 9.2.0 (Bitplane), and the cell properties were imported into Matlab R2016B (MathWorks) from Imaris using the EasyXT [X] package for further analysis using custom scripts. Due to a difference in the average density of T cells for $PD1^-$ versus triple-positive FOVs (111 ± 18 vs. 190 ± 15 T cells/mm^2, t test $P < 0.01$, mean ± SEM), we analyzed only a random subset of triple-positive T cells for each FOV to match the average $PD1^-$ T-cell density of 111 T cells/mm^2. There was no significant difference in the density of tumor cells for $PD1^-$ versus triple-positive FOVs (986 ± 85 vs. 1,137 ± 79, t test $P = 0.22$, mean ± SEM). Only T cells with areas between 50 and 300 μm^2 were analyzed to exclude debris and unhealthy cells. Ca^{2+} spikes were identified as peaks with a prominence exceeding 60% $\Delta F/F$ using the findpeaks Matlab function (https://github.com/PTBIOP/EasyXT).

Single-cell sorting, RNA-seq, and TCR-seq

Established MC38 tumors (~190 mm^3) were excised and single-cell suspensions were stained and sorted into $CD45^+TCR\beta^+$ T cells. Sorted cells were then loaded onto a 10× Chromium Chip A using reagents from the Chromium Single-Cell 5′ Library and Gel Bead Kit (10× Genomics) according to the manufacturer's protocol. Amplified cDNA was used for both 5′ RNA-seq library generation and TCR V(D)J targeted enrichment using the Chromium Single-Cell V(D)J Enrichment Kit for Mouse T Cells (10× Genomics). 5′ RNA-seq and TCR V(D)J libraries were prepared following the manufacturer's user guide (10× Genomics). The final libraries were profiled using the Bioanalyzer High Sensitivity DNA Kit (Agilent Technologies) and quantified using the Kapa Library Quantification Kit (Kapa Biosystems). Each single-cell RNA-seq library was sequenced in one lane of HiSeq4000 (Illumina) to obtain a minimum of 20,000 paired-end reads (26 × 98 bp) per cell. Single-cell TCR V(D)J libraries were multiplexed and sequenced in one lane of HiSeq2500 (Illumina) to obtain minimum of 5,000 paired-end reads (150 × 150 bp) per cell. The sequencing specifications for both single-cell RNA-seq and TCR V(D)J libraries were according to the manufacturer's specification (10× Genomics). The scRNA-seq libraries have been deposited in the ArrayExpress database at EMBL-EBI (www.ebi.ac.uk/arrayexpress) under accession number E-MTAB-7919 and the scTCR sequences have been deposited under accession number E-MTAB-7918.

Processing of single-cell RNA-seq data

Single-cell RNA-seq data for each replicate were processed using cellranger count [CellRanger 2.2.0 (10× Genomics)] using a custom reference package based on mouse reference genome GRCm38 and GENCODE (31) gene models. Individual count tables were merged using cellranger aggr to reduce batch effects. Subsequent data analysis was carried out in R 3.5.1 and the Seurat package version 2.3.4 (32). From an initial set of 6,182 cells, counts of transcripts measured as unique molecule identifiers (UMI) in each cell were normalized and log transformed to log(CPM/100 + 1) [CPM = UMI counts per million]. Cells with at least 800 measured genes per cell were considered for analysis. To remove noise from droplets containing more than one cell, we focused on cells with <5,000 measured genes. Dead cells were excluded by filtering for cells with less than 5% mitochondrial reads leaving 5,654 cells. We further focused our analysis on cells that were positive for either CD8 ($Cd8a^+$ and/or $Cd8b1^+$) or CD4 ($Cd4^+$ and/or $Foxp3^+$) T-cell markers. We obtained data for 1,291–1,759 cells per tumor with a median coverage of ~150,000 5′ RNA-seq reads corresponding to ~8,100 UMI counts per cell. After quality control, 4,036 high-quality T cells were used for downstream analysis. To account for differences in sequencing depth of these 4,036 cells used for final analysis, normalized data were scaled to regress out the number of distinct UMIs. Subsequent to filtering, we used the expression values of the 400 most variable genes to perform a principal component analysis. Principal components 1 to 10 were provided as an input

for dimensionality reduction via Tsne. Clusters of cells were identified based on a shared-nearest neighbor graph between cells and the smart moving (SLM) algorithm ($k = 40$, resolution $= 0.7$).

Processing of single-cell RNA-seq data

TCR sequencing data for each sample were processed using Cell Ranger 2.2.0 software with the command cellranger vdj and the prebuilt mouse reference package, to obtain a possible assignment of a clonotype for each cell, resulting in the output file filtered_contig_annotations.csv. From this file, we extracted the CDR3 consensus protein sequences and considered two cells to have the same clonotype when they shared alpha and beta CDR3 protein sequences. In order to obtain a unique alpha and beta chain assignment for each cell, the following filtering was applied for cells with multiple alpha/beta chains: Only chains with assigned CDR3 nucleotide/protein sequences were retained. If there were still multiple alpha/beta chains in a given cell, only productive chains were retained. In the rare case of multiple productive alpha/beta chains, the chain with the highest UMI counts was chosen as the chain representing the cell.

Statistical analysis

All data were presented as means ± SD except for Fig. 4 (means ± 95% CI). Comparisons between tumor models, time points, treatments, and cell subsets were generated using nonparametric, Mann–Whitney tests. For correlations, two-tailed nonparametric Spearman correlation analysis was used. Prism 6.0 (GraphPad) was used to process all the statistical analyses. Univariate linear regression was performed with R. In Supplementary Table S2, the associations were established and ranked in order to validate the correlation of previously reported biomarkers, as well as the PD-1$^+$LAG3$^+$TIM3$^+$ CTL subset, with anti–PD-L1 response rates. Multiple testing corrections are not commonly applied when validating previous findings (31). Nevertheless, both unadjusted and adjusted *P* values were presented. The latter were obtained using the Benjamini–Hochberg method for multiple testing corrections via FDR estimation.

Results

CD8$^+$ T cells coexpressing inhibitory receptors are highly activated and cytolytic

We first characterized the number and frequency of CD8$^+$ T cells coexpressing the inhibitory receptors PD-1, LAG3, and TIM3 in two commonly used syngeneic murine tumor models responsive to checkpoint blockade: the colon adenocarcinoma MC38 and the breast mammary carcinoma EMT6. Tumor-infiltrating CD8$^+$ T cells were characterized 1 day after tumor establishment. For MC38, this was approximately 19 days after tumor implantation and for EMT6 approximately 9 days. Intratumoral CD8$^+$ T cells showed different frequencies of PD-1, LAG3, and TIM3 coexpression in both tumor models (Fig. 1A; Supplementary Fig. S1A). Both frequencies and absolute numbers of PD-1$^+$ single-positive and PD-1$^+$LAG3$^+$ double-positive CD8$^+$ T cells were higher in MC38 as compared with EMT6 tumors. Although the frequencies of triple-positive cells among CD8$^+$ TILs were comparable in MC38 and EMT6 tumors (Fig. 1A), they were more abundant in absolute numbers in MC38 tumors. The majority of CD8$^+$ T cells in EMT6 tumors were PD-1$^-$ (Fig. 1A; Supplementary Fig. S1B and S1C). However, most of the PD-1$^+$ CD8$^+$ T cells in EMT6 tumors were PD-1$^+$LAG3$^+$TIM3$^+$ triple-positive cells (Supplementary Fig. S1C). In both tumor models, PD-1 expression was higher in CD8$^+$ T cells coexpressing LAG3 and TIM3 (Supplementary Fig. S1D).

We next sought to determine whether the coexpression of inhibitory receptors on CD8$^+$ T cells was associated with a dysfunctional phenotype by evaluating the expression of various activation, cytolytic and functional markers on these cells. The PD-1$^+$LAG3$^+$ (TIM3$^-$) and PD1$^+$LAG3$^+$TIM3$^+$ subsets were enriched in GZMB, Ki-67, ICOS, CD25, and OX40 expressing cells (Fig. 1B; Supplementary Fig. S1E). CD8$^+$ T cells coexpressing PD-1, LAG3, and TIM3 also showed the highest frequency of TIGIT and CD39 expression (Supplementary Fig. S1E) and had the highest frequency of IFNγ$^+$TNFα$^-$ and IFNγ$^+$TNFα$^+$ coexpressing cells following *in vitro* stimulation (Fig. 1C). On a per-cell basis, these cells also expressed the most IFNγ as measured by mean fluorescence intensity (MFI; Fig. 1D).

To confirm whether CD8$^+$ T cells coexpressing inhibitory receptors maintained cytolytic activity, we sorted triple-positive and PD-1$^-$ CD8$^+$ T cells from established MC38 tumors and cultured them with target P815 tumor cells expressing human HER2 and the Ca^{2+} indicator GCaMP6m to read out cytolytic events in real time (32, 33). Target cell killing was triggered by the addition of HER2-TDB (T-cell–dependent bispecific antibody targeting HER2 and CD3; ref. 29) to engage T cells with target cells irrespective of antigen specificity. Tumor-colocalized triple-positive CD8$^+$ T cells led to a higher percentage of Ca^{2+}-spiking in tumor cells when compared with tumor-colocalized PD-1$^-$ T cells (Fig. 1E and F; Supplementary Movies S1 and S2). CD8$^+$ T cells coexpressing inhibitory receptors also showed an increased migratory capacity prior to the addition of HER2-TDB and a larger cell size indicative of a more activated phenotype when compared with PD-1$^-$ cells (Supplementary Fig. S1F and S1G). Taken together, these results indicate that CD8$^+$ T cells coexpressing PD-1, LAG3, and TIM3 represent highly activated, cytotoxic cells, rather than exhausted T cells.

Triple-positive CD8$^+$ T cells are enriched for tumor antigen–specific cells

To determine whether CD8$^+$ T cells coexpressing inhibitory receptors represented antigen experienced cells, we first measured their expression of CD44 and CD62L. In both MC38 and EMT6 tumors, the majority of tumor-infiltrating CD8$^+$ T cells were CD44$^+$CD62L$^-$ effector cells, and this was more evident in cells coexpressing inhibitory receptors (Supplementary Fig. S2A). High expression of the early activation marker CD69 on these cells further suggested recent activation in the tumor (Supplementary Fig. S2B). Using a pool of tetramers derived from immunogenic peptides identified in the MC38 tumor model (34), we determined that tetramer$^+$ cells were mostly PD-1$^+$ and enriched in PD-1$^+$LAG3$^+$TIM3$^+$ triple-positive CD8$^+$ T cells (Fig. 2A). Additionally, following peptide stimulation, triple-positive CD8$^+$ T cells also showed the highest expression of IFNγ, when compared with PD-1$^-$ or PD-1 single-positive T cells (Fig. 2B), suggesting that these cells maintained adequate T-cell receptor (TCR) signaling against tumor antigens despite their high level of inhibitory receptor expression.

To obtain a global and unbiased view of gene expression and TCR usage on CD8$^+$ T cells, we performed combined single-cell 5′ RNA and TCR-sequencing on sorted T cells from four established

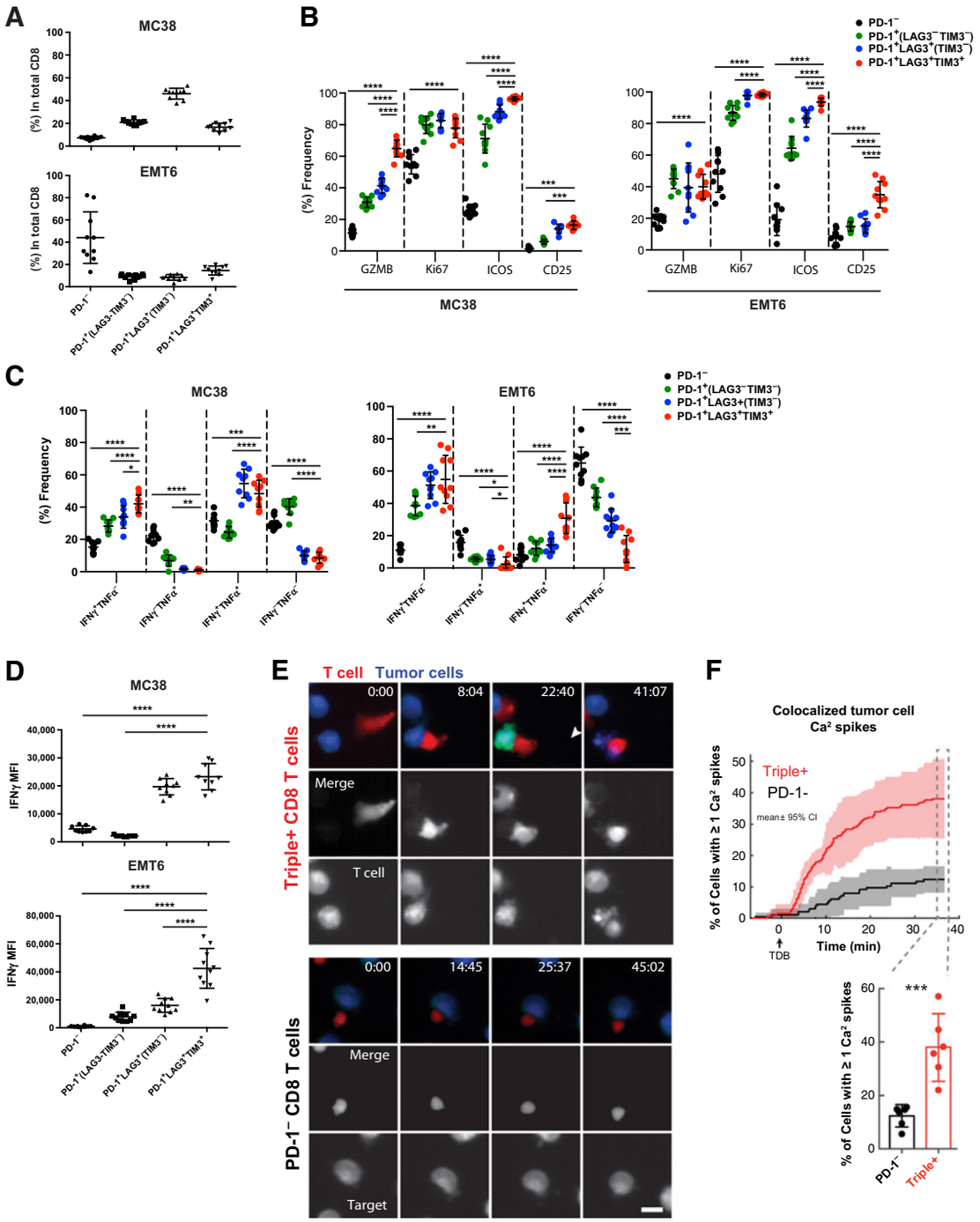

Figure 1.

Tumor-infiltrating CD8$^+$ T cells coexpressing PD-1, LAG3, and TIM3 are highly activated and cytolytic. C57BL/6 and Balb/C mice were inoculated with MC38 and EMT6, respectively, and established tumors were collected to prepare single-cell suspension for flow cytometry analysis. **A,** Frequency of PD-1, LAG3, and TIM3 subsets on intratumoral CD8$^+$ T cells. **B,** Percentage of GZMB, Ki67, ICOS, and CD25 expressing PD-1$^-$ and PD-1$^+$ CD8$^+$ T-cell subsets. **C,** Frequencies of IFNγ and TNFα expressing cells in PD-1 subsets following stimulation with PMA and ionomycin. **D,** MFI for IFNγ in CD8$^+$ T-cell subsets from MC38 and EMT6 tumors. Triple-positive (PD-1$^+$LAG3$^+$TIM3$^+$) and PD-1$^-$PD-1 CD8$^+$ T cells were sorted from established MC38 tumors and placed into wells containing target P815 tumor cells expressing human HER2 and the Ca^{2+} indicator GCaMP6s. T-cell dynamics and tumor cell Ca^{2+} activity was imaged before and after the addition of a HER2-TDB antibody. **E,** Examples of triple-positive and PD-1$^-$ T cells (red) engaging with P815 tumor cells (blue) after HER2-TDB addition at 0 minutes. The tumor cells in the triple-positive example show a Ca^{2+} spike (green) at 22:40 followed by cell death. **F,** Cumulative histogram showing the percentage of T-cell–conjugated tumor cells (<10 μm from a T-cell) with one or more Ca^{2+} spikes versus time for PD-1$^-$ (black) and triple-positive (red) T cells. Bar graph shows the final percentage of cells that have spiked. $N = 6$ FOVs from 2 replicates. Shading and error bars show 95% CI. *, $P < 0.05$; **, $P < 0.01$; ***, $P < 0.001$; ****, $P < 0.0001$.

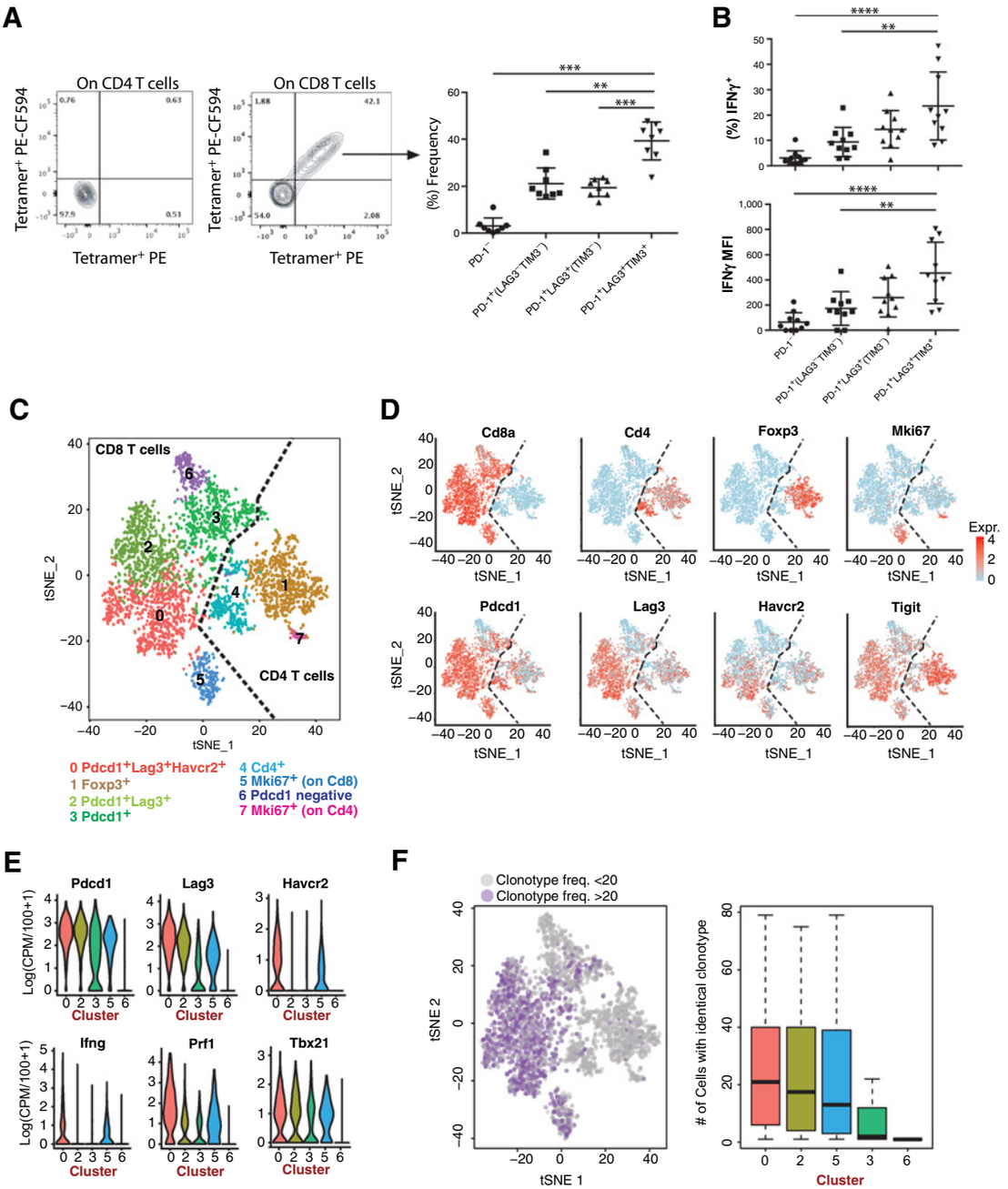

Figure 2.

CD8$^+$ T cells coexpressing inhibitory receptors are enriched in antigen-specific cells and show higher clonality. Established MC38 tumors were collected to prepare single-cell suspensions for flow cytometry analysis. A pool of tetramers specific for immunogenic peptides in the MC38 tumor model were used for staining. **A,** Frequency of tetramer$^+$ cells in CD4$^+$ and CD8$^+$ T cells and PD-1/LAG3/TIM3 subsetting within CD8$^+$ tetramer$^+$ cells. Single-cell suspensions were also stimulated with a peptide pool for 6 hours followed by intracellular staining. **B,** Frequency and MFI of IFNγ in PD-1/LAG3/TIM3 CD8$^+$ T-cell subsets stimulated with the peptide pool. Established MC38 tumors ($N = 4$) were also sorted for single-cell RNA and TCR-seq. **C,** T-distributed stochastic neighbor embedding plot of 4036 cells from TCRb-purified scRNA-seq, colored by cluster membership (cluster 0: $n = 927$ cells; 1: 838, 2:743, 3:709, 4:337, 5:229, 6:212, 7:41). **D,** Embedding as in **C**, colored by the expression of indicated marker genes (top) measured in log (UMI counts per million/100 + 1). **E,** Violin plots of the expression of indicated markers (top) across CD8$^+$ T-cell clusters from (**C**). **F,** Left, embedding as in **C**, purple color marks cells with TCR sequences shared by more than 20 cells. Right, boxplots visualizing the degree of clonal expansion in each CD8$^+$ T-cell cluster from **C**. All pairwise comparisons of clusters 0, 2, 5 vs. 3, 6: adj. $P < 0.01$ (Tukey test). **, $P < 0.01$; ***, $P < 0.001$; ****, $P < 0.0001$.

MC38 tumors. Single-cell transcriptomes allowed for the separation of cells into $CD8^+$ and $CD4^+$ T cells (Fig. 2C and D) across replicates (Supplementary Fig. S2C). Through unsupervised clustering, we identified five subsets of cytotoxic T cells, characterized by different expression of genes encoding coinhibitory receptors, T-cell activation markers as well as markers of proliferation (Fig. 2C–E). T-cell activation markers (e.g., *Ifng*, *Prf1*, and *Tbx21*) were highly enriched (Wilcoxon rank sum test, all adj. $P < 0.001$) in cells marked by elevated expression of coinhibitory receptors (clusters 0, 2, 5; Fig. 2E; Supplementary Fig. S2D).

Using the paired TCR-sequencing data, we sought to understand the clonal structure of the different clusters. Cells with elevated expression of coinhibitory receptors (clusters 0, 2, 5) showed a significantly higher clonality (Turkey test, adj. $P < 0.001$ for all comparisons; Fig. 2F), suggesting that their TCRs are likely tumor antigen–specific. This clonal expansion pattern could at least be partly explained by proliferative T cells at the tumor site ($Mki67^+$ proliferative cluster 5). Together, these results suggest that $CD8^+$ T cells coexpressing inhibitory receptors are enriched in tumor antigen–specific cells characterized by an increased clonality and activation state.

A majority of $CD8^+$ T cells coexpressing inhibitory receptors are T-bet$^+$ and TCF1$^-$

T-bet and EOMES are canonical transcription factors that drive the differentiation of both effector and T_{ex} cells, and have been used to define early and terminal stage Tex cells (35). We examined T-bet and EOMES expression on $CD8^+$ T cells. $CD8^+$ T cells from MC38 and EMT6 tumors displayed distinct patterns of T-bet/EOMES expression, with a higher frequency of $CD8^+$ T cells from MC38 tumors expressing T-bet (T-bet$^+$EOMES$^-$ and T-bet$^+$EOMES$^+$), whereas most $CD8^+$ T cells in EMT6 tumors were T-bet$^-$ (T-bet$^-$EOMES$^+$ and T-bet$^-$EOMES$^-$; Fig. 3A). This difference was likely attributed to differences in PD-1 positivity between the two models: the majority of infiltrating $CD8^+$ T cells in MC38 tumors were PD-1$^+$, and the majority in EMT6 tumors were PD-1$^-$. Indeed, PD-1$^-$ cells in both MC38 and EMT6 tumors were mostly T-bet$^-$, whereas PD-1$^+$ cells were predominantly T-bet$^+$ (Fig. 3B). Additionally, the majority of triple-positive $CD8^+$ T cells were T-bet$^+$ (Fig. 3B). T-bet$^+$ cells also exhibited the highest expression of GZMB, Ki-67 (only for EMT6), ICOS, and IFNγ expression, corroborating their higher activation state (Fig. 3C and D). The majority of circulating $CD8^+$ T cells in blood of MC38 and EMT6 tumor-bearing mice were PD-1$^-$ and were enriched in T-bet$^-$ cells (Supplementary Fig. S3A and S3B). Therefore, incoming $CD8^+$ T cells from the periphery are mostly T-bet$^-$ and likely acquire PD-1 and T-bet expression upon antigen reencounter in the tumor.

Given that TCF1 sustains a stem-like $CD8^+$ T-cell population responsive to anti–PD-1 treatment in chronic LCMV infection, we determined the expression of TCF1 on $CD8^+$ T cells coexpressing inhibitory receptors. PD-1$^+$LAG3$^+$TIM3$^+$ $CD8^+$ T cells showed reduced expression of TCF1 when compared with their PD-1$^-$ counterparts (Fig. 3E), consistent with their higher activation state and effector phenotype (Supplementary Fig. S3C). Additionally, TCF1$^-$ $CD8^+$ T cells encompassed activated triple-positive cells, whereas TCF1$^+$ cells were enriched in less activated PD-1$^-$ cells (Supplementary Fig. S3D). These results show that PD-1$^+$LAG3$^+$TIM3$^+$ $CD8^+$ T cells are more fully differentiated into an effector phenotype and could be more predisposed to exhaustion given sufficient duration of chronic antigenic exposure.

$CD8^+$ T cells coexpressing inhibitory receptors in progressing tumors appear active

The time it takes for MC38 and EMT6 tumors to become established may not be sufficient for tumor-specific T cells to acquire an exhausted phenotype. We therefore sought to address the dynamics of $CD8^+$ T cells in MC38 tumors at later time points when tumors reached an average size of ∼760 and 1600 mm^3 (6 and 13 days after establishment). Total $CD8^+$ T-cell density decreased with time as tumor volume increased (Fig. 4A). The frequency of PD-1$^+$LAG3$^+$TIM3$^+$ $CD8^+$ T cells decreased slightly over time with minor accumulation of PD-1 single positive and PD-1$^-$ T cells (Fig. 4B). This could be due to reduced differentiation of $CD8^+$ T cells into triple-positive cells or impaired proliferation, defective maintenance, or increased apoptosis of these cells. However, we did not observe decreased Bcl2 in cells coexpressing inhibitory receptors (Fig. 4C) and Ki-67 expression was generally maintained over time (Fig. 4D). GZMB production was also maintained between days 1 and 13 (Fig. 4E). Nonetheless, the total fraction of IFNγ$^+$ $CD8^+$ T cells fell significantly as tumors progressed (Fig. 4F). However, when compared with cytokine expression from $CD8^+$ T-cell subsets at baseline (Fig. 1C), triple-positive T cells still retained the highest expression of IFNγ compared with PD-1 single-positive or PD-1$^-$ $CD8^+$ T cells (Fig. 4G). TNFα expression increased with time in every $CD8^+$ T-cell subset with high expression observed in the PD-1$^-$ subset. These observations suggest that $CD8^+$ T cells undergo a decline in abundance and polyfunctionality as tumors progress, with an accumulation of less activated PD-1$^-$ cells. Regardless of these changes, $CD8^+$ T cells coexpressing inhibitory receptors were enriched in Ki-67, GZMB, and IFNγ expression and therefore represented activated rather than exhausted cells.

Anti–PD-L1 increases the number of $CD8^+$ T cells coexpressing inhibitory receptors

Given that inhibitory receptors such as PD-1 can reduce the functional capacity of T cells following ligand engagement, we measured PD-L1 expression in MC38 and EMT6 tumors. Both tumor models showed high PD-L1 expression in the hematopoietic (CD45$^+$) and nonhematopoietic (CD45$^-$) compartments (Supplementary Fig. S4A), which can partly explain why, despite being infiltrated by activated PD-1$^+$ $CD8^+$ T cells, these tumors continue to grow. We thus hypothesized that anti–PD-L1 treatment could not only increase the number, but also further enhance the functionality of PD-1$^+$ cells. As shown in Fig. 5A, MC38 and EMT6 tumors partially responded to anti–PD-L1 treatment, resulting in 12% and 20% complete responses, respectively, with a delay in tumor growth in the majority of tumor-bearing mice. We next examined tumor infiltrates 7 days after treatment initiation and found that anti–PD-L1 treatment significantly expanded the population of triple-positive $CD8^+$ T cells in both tumor models (Fig. 5B), while increasing the frequency of GZMB and ICOS expressing $CD8^+$ T cells (Supplementary Fig. S4B and S4C). Using the same pool of tetramers to detect antigen-specific T cells in the MC38 tumor model, we found that anti–PD-L1 treatment increased the absolute number of antigen-specific cells in tumors, suggesting an increase in $CD8^+$ effector cell function and not simply increased rates of

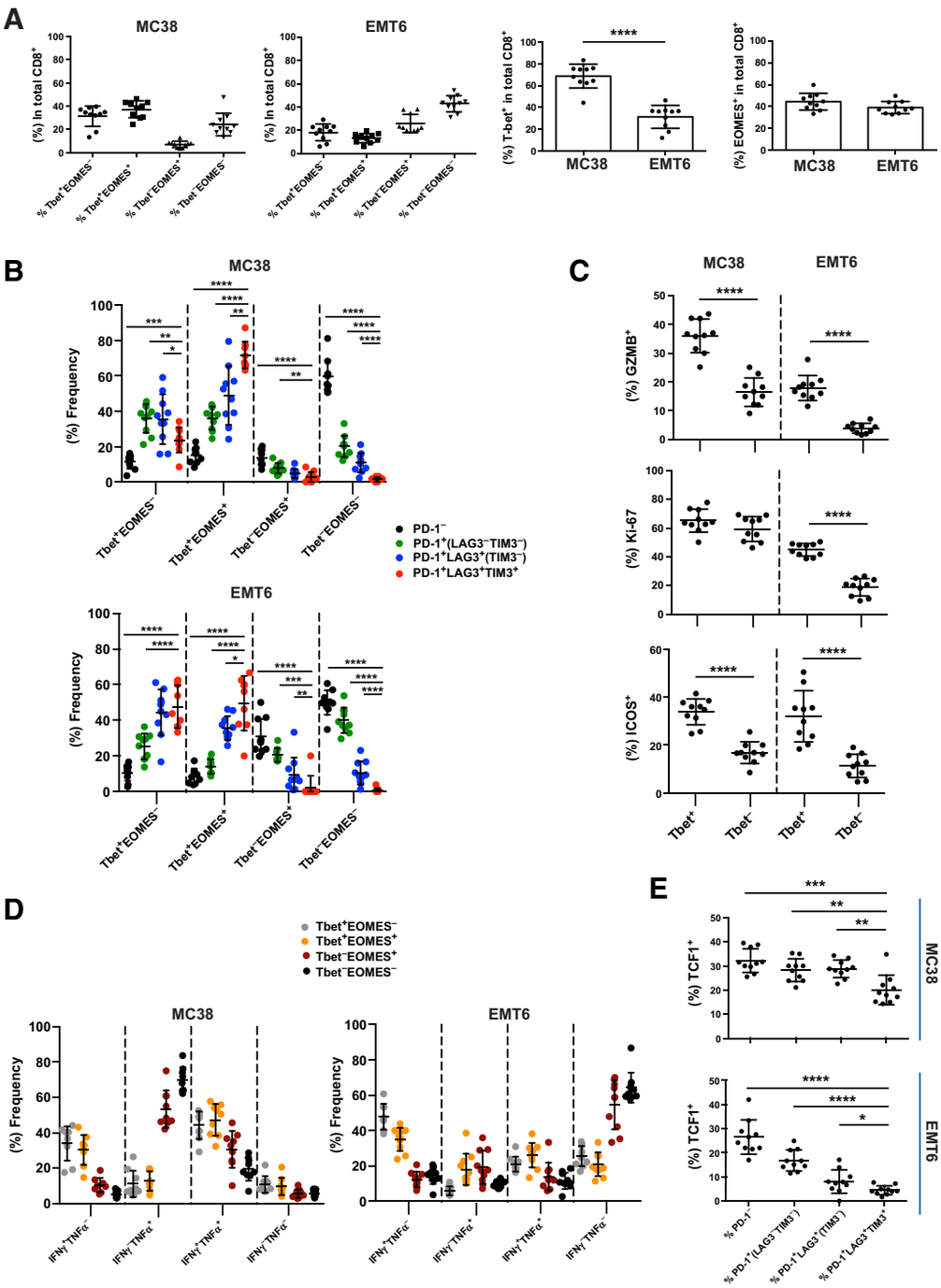

Figure 3.
A majority of CD8$^+$ T cells coexpressing inhibitory receptors are T-bet$^+$. **A,** Frequencies of T-bet/EOMES subsets in total CD8$^+$ T cells from MC38 (left) and EMT6 (middle) tumors; frequency of T-bet$^+$ (T-bet$^+$EOMES$^-$ and T-bet$^+$EOMES$^+$) populations in total CD8$^+$ T cells (right). **B,** Percentages of T-bet/EOMES subsets in PD-1/LAG3/TIM3 expressing CD8$^+$ T cells. **C,** Frequency of GZMB, Ki-67, and ICOS expression in T-bet$^+$ and T-bet$^-$ CD8$^+$ T cells. **D,** Percentages of IFNγ/TNFα subsets within T-bet/EOMES subsets in CD8$^+$ T cells. **E,** Frequency of TCF1$^+$ cells in CD8 PD1 subsets. *, $P < 0.05$; **, $P < 0.01$; ***, $P < 0.001$; ****, $P < 0.0001$.

differentiation into activated cells (Fig. 5C). PD-1$^-$CD8$^+$ T cells did not expand following treatment, but they exhibited an increase in ICOS and GZMB expression (MC38 and EMT6 tumors, respectively), likely through secondary mechanisms (Fig. 5B; Supplementary Fig. S4B and S4C). These results demonstrate that CD8$^+$ T cells coexpressing inhibitory receptors are responsive to anti–PD-L1 treatment and that despite being highly activated, inhibitory signaling through PD-1 can reduce

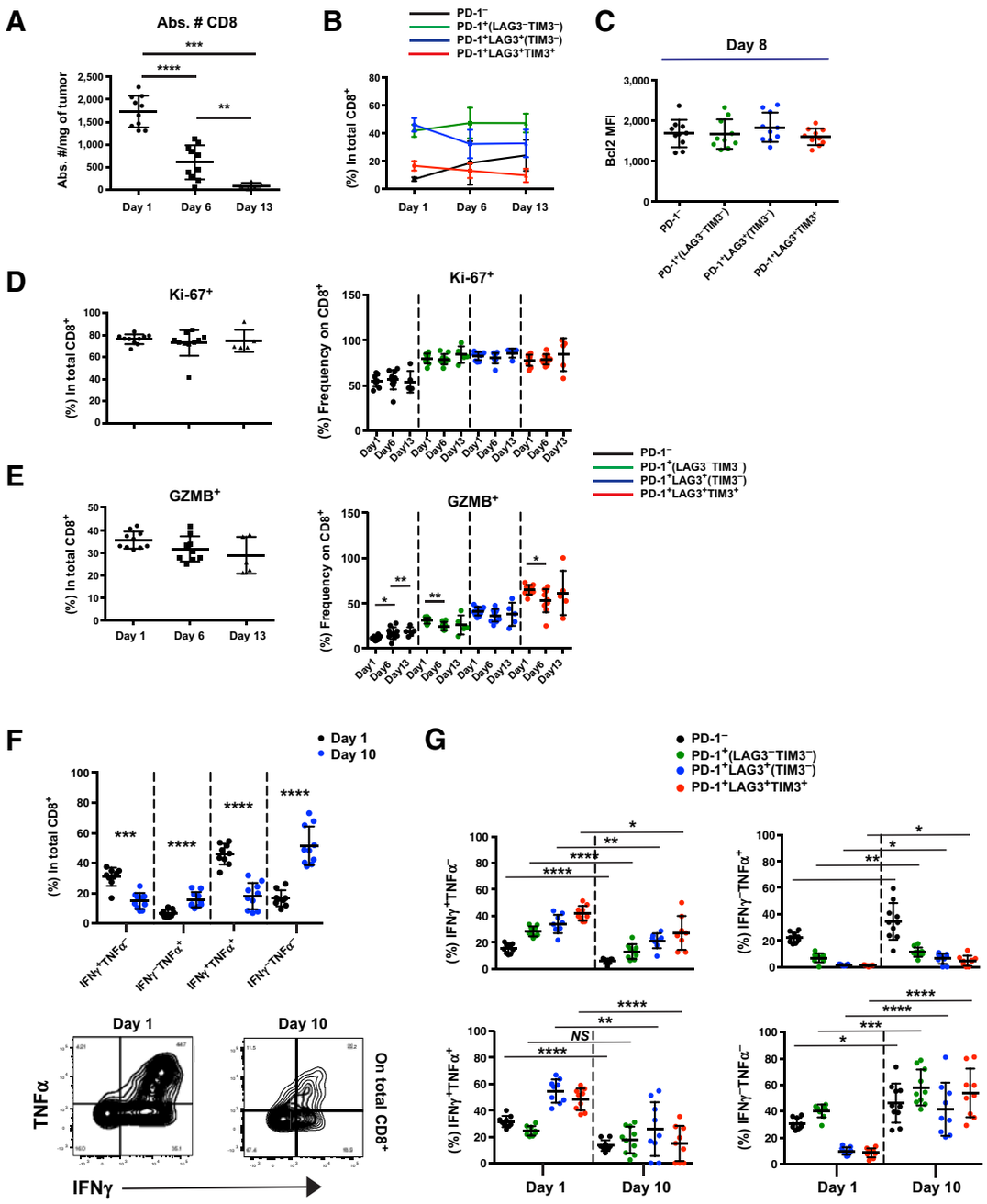

Figure 4.

Overall decrease in IFNγ output with time on total CD8$^+$ T cells but no evidence of augmented dysfunction in PD-1/LAG3/TIM3 subsets. **A–E,** MC38 tumors were collected 1 day after they became established at an average size of ∼180 mm^3 followed by 6 (∼760 mm^3) and 13 (∼1600 mm^3) days later. **A,** Absolute number (cells/mg of tumor) of CD8$^+$ T cells at different time points. **B,** Change in the frequency of PD-1$^+$ subsets with time. **C,** MFI for Bcl2 on PD-1/LAG3/TIM3 subsets. **D,** Change in the frequency of Ki67 and (**E**) GZMB expressing cells among total CD8 (left) and PD-1 subsets (right). **F** and **G,** Maximal cytokine output on total CD8$^+$ T cells was assessed by PMA and ionomycin stimulation 1 day after tumors reached ∼180 mm^3 and on day 10. **F,** Changes in the frequency of IFNγ and TNFα producing cells in total CD8$^+$ T cells. **G,** Change in the frequency of IFNγ and TNFα expressing cells within PD-1 subsets. Baseline results from day 1 are taken from Fig. 1C for comparison with day 10. *, $P < 0.05$, **, $P < 0.01$; ***, $P < 0.001$; ****, $P < 0.0001$.

their overall functional output.esponse to anti–PD-L1 treatment and coexpression of inhibitory receptors.

Having observed an increase in the number and activation state of triple-positive CD8$^+$ T cells in MC38 and EMT6 tumors following anti–PD-L1 treatment, we next assessed whether the abundance of these cells correlated with response to treatment. To this end, we analyzed two additional tumor models, both of mammary origin (JC and 4T1) and refractory to anti–PD-L1

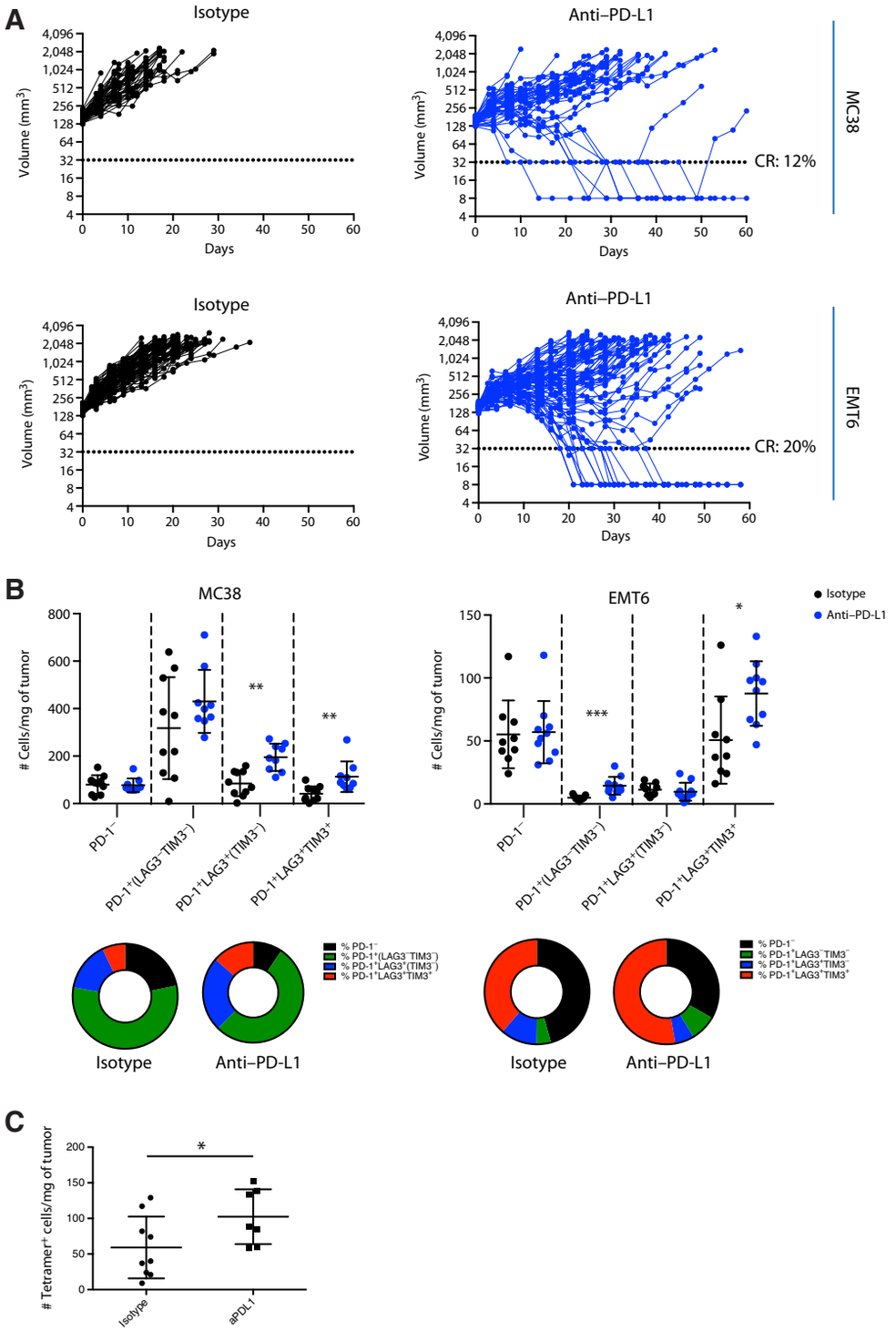

Figure 5.

Anti–PD-L1 treatment increases the number and activity of $CD8^+$ T cells coexpressing inhibitory receptors in responsive MC38 and EMT6 tumors. Mice were inoculated with either MC38 or EMT6 tumor cells and once tumors became established at ~180 mm^3 (day 0) mice with similarly sized tumors were grouped into treatment arms. The next day (day 1) mice were dosed with anti–PD-L1 or isotype control antibody at 10 mg/kg (i.v.) for the first dose and 5 mg/kg (i.p.) thereafter twice a week for 3 weeks. Tumors were collected 7 days after treatment initiation, digested, and single-cell suspensions used for FACS analysis. **A,** Tumor volume (mm^3) of control and anti–PD-L1-treated mice shown on a $\log_2$ scale. Tumor volumes below 32 mm^3 (dotted line) indicate complete responses. **B,** Absolute numbers (cells/mg of tumor) of PD-1 subsets in $CD8^+$ T cells from control or anti–PD-L1-treated MC38 (left) or EMT6 (right) tumor-bearing mice. Pie charts depict the average proportion of PD-1/LAG3/TIM3 subsets within total $CD8^+$ T cells. **C,** The absolute number of antigen-specific cells per mg of tumor as measured by tetramer staining in MC38 7 days after treatment initiation. *, $P < 0.05$; **, $P < 0.01$; ***, $P < 0.001$.

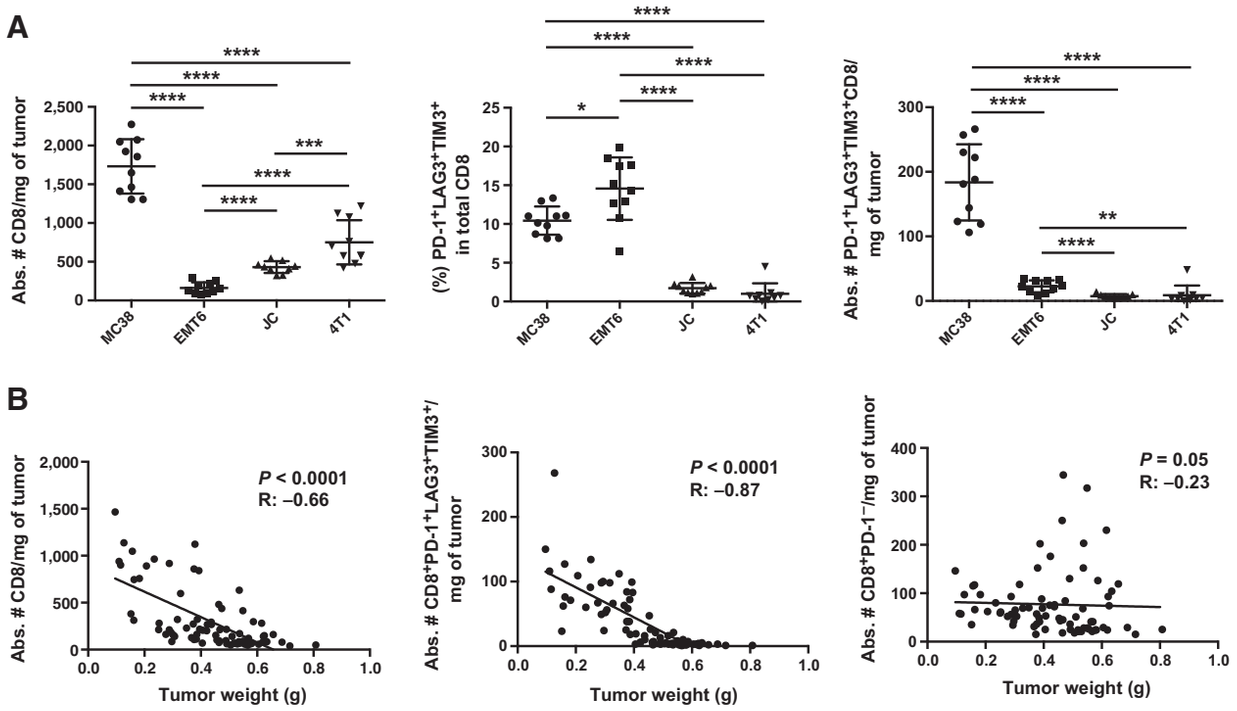

Figure 6.

Baseline abundance of CD8$^+$ T cells coexpressing inhibitory receptors correlates with response to anti–PD-L1 treatment. **A,** Absolute number of total and PD-1$^+$LAG3$^+$TIM3$^+$ CD8$^+$ T cells and in anti–PD-L1 responsive (MC38 and EMT6) and nonresponsive (JC and 4T1) tumor models. **B,** Correlation between the absolute number/mg of tumor of total, PD-1$^+$LAG3$^+$TIM3$^+$ or PD-1$^-$ CD8$^+$ T cells and tumor weight. Correlation plots were generated by pooling data from MC38, EMT6, JC, and 4T1 tumor models 7 days after treatment initiation. *, $P < 0.05$; **, $P < 0.01$; ***, $P < 0.001$; ****, $P < 0.0001$.

treatment (Supplementary Fig. S5). Inspection of CD8$^+$ TILs in established tumors prior to treatment revealed fewer PD-1$^+$LAG3$^+$TIM3$^+$ CD8$^+$ T cells in JC and 4T1 tumors than in tumors from MC38 and EMT6 (Fig. 6A; Supplementary Fig. S6A), despite the latter two models having higher numbers of total CD8$^+$ TILs compared with EMT6. Similar to our observations in MC38 and EMT6 tumors, triple-positive TILs from JC and 4T1 tumors showed the highest expression of GZMB and Ki-67 (Supplementary Fig. S6B and S6C) and, in JC tumors, the highest expression of IFNγ (Supplementary Fig. S6D and S6E). In 4T1, IFNγ output was highest in the PD-1$^+$LAG3$^+$TIM3$^-$ subset, suggesting that in this tumor model, triple-positive CD8$^+$ TILs might be entering an initial stage of dysfunction relative to the other PD-1 subsets.

Across all four models, the number of CD8$^+$ TILs showed a negative correlation with tumor weight in control and anti–PD-L1–treated tumors (Fig. 6B). However, this negative correlation was more pronounced for triple-positive CD8$^+$ TILs, whereas there was little correlation between numbers of PD-1$^-$ CD8$^+$ TILs and tumor weight (Fig. 6B). Together, these results suggest that although in nonresponsive tumor models other mechanisms seem to prevent the generation of triple-positive TILs, PD-1$^+$ cells still represent highly activated CD8$^+$ T cells, whose numbers are positively correlated with response to treatment.

The connection between triple-positive T cells and responsiveness to anti–PD-L1 treatment prompted us to expand this investigation into nine additional syngeneic tumor models. A range of response rates were recorded among the 13 tumor models, measured as the percentage of tumor growth inhibition (% TGI) relative to the isotype control group (Table 1). We generated extensive flow cytometry panels and measured an expansive list of parameters at the time of tumor establishment, thereby normalizing tumor burden and obtaining a baseline characterization for all the tumor models investigated. A variety of common immune infiltrates and phenotypic markers from tumor, draining lymph nodes (dLN), and blood (Supplementary Table S1) were included in the staining panels. We then performed a univariate

Table 1. % TGI after anti–PD-L1 treatment in different syngeneic tumor models

Tumor model	(%) TGI
Hepa1-6 × 1	104
Cloudman S91	95
EMT6	73
MC38	71
A20	69
EG7	30
CT26	21
JC	11
SM1	11
EL4	9
4T1	6
LLC	0
AB22	0

NOTE: Response rates of different syngeneic tumor models to anti–PD-L1 treatment, shown as the % of TGI, defined as (1 – (mean volume of treated tumors)/(mean volume of control tumors)) × 100 when compared with the isotype control group.

linear regression analysis to validate which parameters associated with response to treatment. Due to the practical limitation of the number of available tumor models, most parameters did not reach statistical significance (adj. $P < 0.05$), but there was a significant and positive correlation between the PD-1$^+$LAG3$^+$TIM3$^+$ CD8$^+$/Treg ratio and response to anti–PD-L1 (Supplementary Table S2). Previously reported biomarkers, such as Ki-67 expression on CD8$^+$ TILs and PD-L1 expression, were among the top positive parameters associated with response to treatment, whereas the frequency of PD-1$^-$ CD8$^+$ T cells had a negative association (13, 14, 17). Additionally, the density and activation phenotypes of PD-1$^+$LAG3$^+$TIM3$^+$ CD8$^+$ TILs positively correlated with response, making up half of the top correlates (Supplementary Table S2, arrows). Despite having adjusted *P* values higher than 0.05, the enrichment of multiple factors related to PD-1$^+$LAG3$^+$TIM3$^+$ CD8$^+$ T cells suggests that these cells are relevant for antitumor responses following anti–PD-L1 treatment. Collectively, these results confirm that the relative abundance of CD8$^+$ T cells coexpressing inhibitory receptors in tumors correlates with response to anti–PD-L1 treatment, reflecting overall CD8$^+$ T-cell activation and not necessarily T-cell exhaustion.

Discussion

T-cell functionality and exhaustion states may serve as predictive and prognostic determinants of anti–PD-1/PD-L1 treatment. Understanding which cell subsets can be reinvigorated by checkpoint inhibitors can bolster our understanding of the mechanism of action of such therapies and help develop better strategies to improve responses in cancer patients. In this study, we have shown that in different syngeneic tumor models, CD8$^+$ T cells coexpressing inhibitory receptors are not exhausted, but rather represent highly activated and functional effector cells. These cells express GZMB, Ki-67, ICOS, CD25, OX40, CD44, IFNγ, and T-bet and their abundance correlates with reduced tumor burden and response to anti–PD-L1 treatment. This does not contradict the notion that in the tumor microenvironment, PD-1, LAG3, and TIM3 engagement can reduce the functional capacity of PD-1$^+$LAG3$^+$TIM3$^+$ CD8$^+$ T cells. Rather, checkpoint blockade can maintain or enhance the functionality of these activated CTLs by blocking their inhibitory signaling. These findings are in line with a report showing an increased in PD-1$^+$TIM3$^+$T-bet$^+$EOMES$^{+/-}$ T cells following anti–PD-1 and anti–CTLA-4 treatment in MC38 and B16BL6 tumor models (36). In contrast, PD-1$^-$ cells that showed reduced activation were mostly T-bet$^-$ and their T-bet/EOMES phenotype was more similar to circulating blood CD8$^+$ T cells; hence, this subset could be largely composed of cells that are not activated or specific for tumor antigen. Indeed, antigen-specific T cells in MC38 tumors were enriched in triple-positive CD8$^+$ T cells and were mostly absent in the PD-1$^-$ subset. This was also observed in melanoma patient tumors were CD8$^+$ T cells defined as exhausted based on their expression of inhibitory gene signatures were actually highly proliferative and clonal (37). PD-1 expression therefore likely coincides with and reflects T-cell activation in the tumor.

If PD-1 expression is a determinant of T-cell activation in the tumor, it is likely that triple-positive CD8$^+$ T cells represent clones undergoing high-avidity TCR interactions, resulting in increased inhibitory receptor expression (38). Indeed, triple-positive CD8$^+$ T cells showed increased antigen specificity, higher clonality, and higher PD-1 and CD69 expression relative to the other PD-1 subsets, suggesting stronger and continuous TCR signaling (39). Additionally, triple-positive cells also showed increased expression of CD8 coreceptor, which has been shown to function as a positive regulator by decreasing the activation threshold of cells (40). Triple-positive cells are therefore likely undergoing strong TCR interactions, resulting in their highly activated state that is characterized by the coexpression of various inhibitory receptors. These are probably required to ensure that there is always appropriate ligand present to control their high cytolytic potential.

High T-bet and low TCF1 expression of triple-positive CD8$^+$ T cells suggest that these cells represent more terminally differentiated effector cells. Syngeneic tumor models, which generally encompass only a few weeks of tumor growth, are likely more representative of an early onset chronic infection, which can be characterized by increased expression of TCF1$^-$ and highly activated CD8$^+$ T cells that coexpress multiple inhibitory receptors, as described (41). However, an outstanding question is whether these cells truly become exhausted in the tumor setting where microenvironmental factors likely differ from chronic viral infection models. Furthermore, dysfunction in a tumor context could also be transcriptionally and phenotypically distinct. In human cancers, where the chronicity of tumor growth is longer compared with mouse model systems, the effect of Tex cells may differ.

Prior work in slow-growing prostate TRAMP-C2 and ASTxCre-ER^{T2} autochthonous liver murine cancer models showed that intratumoral PD-1^{hi} CD8$^+$ T cells collected 35–45 days after tumor inoculation acquired a stable state of DNA-methylation and epigenetic modifications associated with exhaustion (42, 43). Evidence in non–small cell lung cancer patients suggested that similar to our observations in syngeneic tumor models, the presence of PD-1^{hi} CD8$^+$ T cells, which also coexpressed LAG3, TIM3 as well as other inhibitory and activation markers, correlated with increased overall survival, and durable responses (36, 44). Although PD-1^{hi} CD8$^+$ T cells showed reduced expression of effector cytokines and metabolic dysregulation, their dysfunctional state was distinct from that described in chronic viral infection models, reinforcing the idea that the tumor context imparts different signaling on CD8$^+$ T cells.

It is therefore plausible that CD8$^+$ T cells coexpressing inhibitory receptors represent a heterogeneous population of both activated and dysfunctional or exhausted cells depending on parameters such as their microanatomical niche in the tumor tissue, which could affect the quality of antigen presentation and cytokine signaling, the presence of other suppressive factors as well as antigenic exposure. Moreover, it is possible that the majority of triple-positive cells are too short lived to become exhausted, unless encountering the right microenvironmental conditions. In this case, checkpoint inhibitors could be acting to preserve the activity of effector cells as we observed in our tumor models. Although most syngeneic murine tumor models represent only the early onset of tumor growth, it is conceivable that the dynamics of T-cell infiltration in human tumors will encompass multiple rounds of cell death and priming as well as effector cell recruitment; thus, anti–PD-1/PD-L1 treatment could also be preventing the functional suppression of effector cells even in a tumor setting of longer establishment. Although other T-cell populations such as memory cells could also be affected by checkpoint inhibitors, our mouse tumor studies showed that activated triple-positive effector cells direct the response to anti–PD-L1 treatment. The degree of inhibitory receptor

expression on intratumoral CD8$^+$ T cells can therefore be associated with an increased activation state such that higher activation coincides with increased expression of multiple inhibitory receptors.

Disclosure of Potential Conflicts of Interest

H. Xiong has ownership interest (including stock, patents, etc.) in Genentech. S. Mittman has ownership interest (including stock, patents, etc.) in Genentech. R. Rodriguez has ownership interest (including stock, patents, etc.) in Genentech. P. Pacheco-Sanchez has ownership interest (including stock, patents, etc.) in Genentech. S. Müller has ownership interest (including stock, patents, etc.) in Genentech Inc. D. Nickles has ownership interest (including stock, patents, etc.) in Genentech. A.-H. Capietto is a senior scientific researcher at Genentech and reports receiving a commercial research grant from the same. L. Delamarre has ownership interest (including stock, patents, etc.) in Genentech. S. Rutz has ownership interest (including stock, patents, etc.) in Genentech. I. Mellman is Vice President at, reports receiving a commercial research grant from, and has ownership interest (including stock, patents, etc.) in Genentech. R. Cubas has ownership interest (including stock, patents, etc.) in Genentech. No potential conflicts of interest were disclosed by the other authors.

Authors' Contributions

Conception and design: H. Xiong, I. Mellman, R. Cubas
Development of methodology: H. Xiong, A.T. Ritter, A.-H. Capietto, L. Delamarre, R. Cubas
Acquisition of data (provided animals, acquired and managed patients, provided facilities, etc.): H. Xiong, S. Mittman, R. Rodriguez, P. Pacheco-Sanchez, M. Moskalenko, Y. Yang, A.T. Ritter, T.L. Arenzana, Z. Modrusan, R. Cubas
Analysis and interpretation of data (e.g., statistical analysis, biostatistics, computational analysis): H. Xiong, S. Mittman, R. Rodriguez, P. Pacheco-Sanchez, M. Moskalenko, Y. Yang, J. Elstrott, A.T. Ritter, S. Müller, D. Nickles, I. Mellman, R. Cubas
Writing, review, and/or revision of the manuscript: H. Xiong, M. Moskalenko, J. Elstrott, D. Nickles, A.-H. Capietto, L. Delamarre, S. Rutz, I. Mellman, R. Cubas
Administrative, technical, or material support (i.e., reporting or organizing data, constructing databases): R. Rodriguez, S. Rutz, R. Cubas
Study supervision: R. Cubas

Acknowledgments

We would like to thank Sophie Lehar for her support with the tetramer staining protocol. The authors would also like to thank the core dosers at Genentech as well as the cell line core group for their contribution to this project. We would also like to thank the flow cytometry core group for their help with cell sorting. All work was funded by and conducted at Genentech.

The costs of publication of this article were defrayed in part by the payment of page charges. This article must therefore be hereby marked *advertisement* in accordance with 18 U.S.C. Section 1734 solely to indicate this fact.

Received October 18, 2018; revised January 31, 2019; accepted April 18, 2019; published first May 7, 2019.

References

1. Wherry EJ. T cell exhaustion. Nat Immunol 2011;12:492–9.
2. Sen D, Kaminski J, Barnitz R, Kurachi M, Gerdemann U, Yates K, et al. The epigenetic landscape of T cell exhaustion. Science 2016;354:1165–9.
3. Pauken K, Sammons M, Odorizzi P, Manne S, Godec J, Khan O, et al. Epigenetic stability of exhausted T cells limits durability of reinvigoration by PD-1 blockade. Science 2016;354:1160–5.
4. Wherry EJ, Ha SJ, Kaech SM, Haining WN, Sarkar S, Kalia V, et al. Molecular signature of CD8+ T cell exhaustion during chronic viral infection. Immunity 2007;27:670–84.
5. Blackburn SD, Shin H, Haining WN, Zou T, Workman CJ, Polley A, et al. Coregulation of CD8+ T cell exhaustion by multiple inhibitory receptors during chronic viral infection. Nat Immunol 2009;10:29–37.
6. Jin HT, Anderson AC, Tan WG, West EE, Ha SJ, Araki K, et al. Cooperation of Tim-3 and PD-1 in CD8$^+$ T-cell exhaustion during chronic viral infection. Proc Natl Acad Sci U S A 2010;107:14733–8.
7. Day CL, Kaufmann DE, Kiepiela P, Brown JA, Moodley ES, Reddy S, et al. PD-1 expression on HIV-specific T cells is associated with T-cell exhaustion and disease progression. Nature 2006;443:350–4.
8. Paley MA, Kroy DC, Odorizzi PM, Johnnidis JB, Dolfi DV, Barnett BE, et al. Progenitor and terminal subsets of CD8+ T cells cooperate to contain chronic viral infection. Science 2012;338:1220–5.
9. Fourcade J, Sun Z, Benallaoua M, Guillaume P, Luescher IF, Sander C, et al. Upregulation of Tim-3 and PD-1 expression is associated with tumor antigen-specific CD8+ T cell dysfunction in melanoma patients. J Exp Med 2010;207:2175–86.
10. Kao C, Oestreich K, Paley M, Crawford A, Angelosanto J, Ali MA, et al. Transcription factor T-bet represses expression of the inhibitory receptor PD-1 and sustains virus-specific CD8+ T cell responses during chronic infection. Nat Immunol 2011;12:663–671.
11. Philip M, Fairchild L, Sun L, Horste E, Camara S, Shakiba M, et al. Chromatin states define tumour-specific T cell dysfunction and reprogramming. Nature 2017;545:452–6.
12. Wherry E, Kurachi M. Molecular and cellular insights into T cell exhaustion. Nat Rev Immunol 2015;15:486–499.
13. Powles T, Eder JP, Fine GD, Braiteh FS, Loriot Y, Cruz C, et al. MPDL3280A (anti-PD-L1) treatment leads to clinical activity in metastatic bladder cancer. Nature 2014;515:558–62.
14. Herbst RS, Soria JC, Kowanetz M, Fine GD, Hamid O, Gordon MS, et al. Predictive correlates of response to the anti-PD-L1 antibody MPDL3280A in cancer patients. Nature 2014;515:563–7.
15. Brahmer J, Tykodi S, Chow L, Hwu WJ, Topalian S, Hwu P, et al. Safety and activity of anti–PD-L1 antibody in patients with advanced cancer. N Engl J Med 2012;366:2455–65.
16. Zou W, Wolchok JD, Chen L. PD-L1 (B7-H1) and PD-1 pathway blockade for cancer therapy: mechanisms, response biomarkers, and combinations. Sci Transl Med 2016;8:328rv4.
17. Huang A, Postow M, Orlowski R, Mick R, Bengsch B, Manne S, et al. T-cell invigoration to tumour burden ratio associated with anti-PD-1 response. Nature 2017;545:60–5.
18. Im S, Hashimoto M, Gerner M, Lee J, Kissick H, Burger M, et al. Defining CD8+ T cells that provide the proliferative burst after PD-1 therapy. Nature 2016;537:417–21.
19. Sakuishi K, Apetoh L, Sullivan J, Blazar B, Kuchroo V, Anderson A. Targeting Tim-3 and PD-1 pathways to reverse T cell exhaustion and restore anti-tumor immunity. J Exp Med 2010;207:2187–94.
20. Woo SR, Turnis M, Goldberg M, Bankoti J, Selby M, Nirschl C, et al. Immune inhibitory molecules LAG-3 and PD-1 synergistically regulate T-cell function to promote tumoral immune escape. Cancer Res 2012;72:917–27.
21. Agata Y, Kawasaki A, Nishimura H, Ishida Y, Tsubat T, Yagita H, et al. Expression of the PD-1 antigen on the surface of stimulated mouse T and B lymphocytes. Int Immunol 1996;8:765–72.
22. Vibhakar R, Juan G, Traganos F, Darzynkiewicz Z, Finger LR. Activation-induced expression of human programmed death-1 gene in T-lymphocytes. Exp Cell Res 1997;232:25–8.
23. Freeman GJ, Long AJ, Iwai Y, Bourque K, Chernova T, Nishimura H, et al. Engagement of the PD-1 immunoinhibitory receptor by a novel B7 family member leads to negative regulation of lymphocyte activation. J Exp Med 2000;192:1027–34.
24. Gros A, Robbins P, Yao X, Li Y, Turcotte S, Tran E, et al. PD-1 identifies the patient-specific CD8+ tumor-reactive repertoire infiltrating human tumors. J Clin Invest 2014;124:2246–59.
25. Williams J, Horton B, Zheng Y, Duan Y, Powell J, Gajewski T. The EGR2 targets LAG-3 and 4-1BB describe and regulate dysfunctional antigen-specific CD8$^+$ T cells in the tumor microenvironment. J Exp Med 2017;214:381–400.

26. Ganesan AP, Clarke J, Wood O, Garrido-Martin E, Chee S, Mellows T, et al. Tissue-resident memory features are linked to the magnitude of cytotoxic T cell responses in human lung cancer. Nat Immunol 2017;18: 940–50.
27. Milner J, Toma C, Yu B, Zhang K, Omilusik K, Phan A, et al. Runx3 programs CD8+ T cell residency in non-lymphoid tissues and tumours. Nature 2017; 552:253–7.
28. Singer M, Wang C, Cong L, Marjanovic ND, Kowalczyk MS, Zhang H, et al. A distinct gene module for dysfunction uncoupled from activation in tumor-infiltrating T cells. Cell 2016;166:1500–11.
29. Junttila T, Li J, Johnston J, Hristopoulos M, Clark R, Ellerman D, et al. Antitumor efficacy of a bispecific antibody that targets HER2 and activates T cells. Cancer Res 2014;74:5561–71.
30. Chen TW, Wardill TJ, Sun Y, Pulver SR, Renninger SL, Baohan A, et al. Ultrasensitive fluorescent proteins for imaging neuronal activity. Nature 2013;499:295–300.
31. Trachtenberg E, Korber B, Sollars C, Kepler T, Hraber P, Hayes E, et al. Advantage of rare HLA supertype in HIV disease progression. Nat Med 2003;9:928–35.
32. Ritter A, Kapnick S, Murugesan S, Schwartzberg P, Griffiths G, Lippincott-Schwartz J. Cortical actin recovery at the immunological synapse leads to termination of lytic granule secretion in cytotoxic T lymphocytes. Proc Natl Acad Sci U S A 2017;114:E6585–94.
33. Halle S, Keyser KA, Stahl FR, Busche A, Marquardt A, Zheng X, et al. In vivo killing capacity of cytotoxic T cells is limited and involves dynamic interactions and T cell cooperativity. Immunity 2016;44:233–45.
34. Yadav M, Jhunjhunwala S, Phung Q, Lupardus P, Tanguay J, Bumbaca S, et al. Predicting immunogenic tumour mutations by combining mass spectrometry and exome sequencing. Nature 2014;515:572.
35. Doering TA, Crawford A, Angelosanto JM, Paley MA, Ziegler CG, Wherry EJ. Network analysis reveals centrally connected genes and pathways involved in CD8+ T cell exhaustion versus memory. Immunity 2012; 37:1130–44.
36. Wei SC, Levine JH, Cogdill AP, Zhao Y, Anang NAS, Andrews MC, et al. Distinct cellular mechanisms underlie anti-CTLA-4 and anti-PD-1 checkpoint blockade. Cell 2017;170:1120–33.
37. Li H, Leun A, Yofe I, Lubling Y, Gelbard-Solodkin D, Akkooi A, et al. Dysfunctional $CD8^+$ T cells form a proliferative, dynamically regulated compartment within human melanoma. Cell 2019;176:775–89.
38. Zahm C, Colluru V, McNeel D. Vaccination with high-affinity epitopes impairs antitumor efficacy by increasing PD-1 expression on $CD8^+$ T cells. Cancer Immunol Res 2017;5:630–41.
39. Bally A, Austin J, Boss J. Genetic and epigenetic regulation of PD-1 expression. J Immunol 2016;196:2431–7.
40. Feinerman O, Veiga J, Dorfman J, Germain R, Altan-Bonnet G. Variability and robustness in T cell activation from regulated heterogeneity in protein levels. Science 2008;321:1081–4.
41. Snell L, MacLeod B, Law J, Osokine I, Elsaesser H, Hezaveh K, et al. CD8+ T cell priming in established chronic viral infection preferentially directs differentiation of memory-like cells for sustained immunity. Immunity 2018;49:678–94.
42. Ghoneim H, Fan Y, Moustaki A, Abdelsamed H, Dash P, Dogra P, et al. De novo epigenetic programs inhibit PD-1 blockade-mediated T cell rejuvenation. Cell 2017;170:142–57.
43. Schietinger A, Philip M, Krisnawan VE, Chiu EY, Delrow JJ, Basom RS, et al. Tumor-specific T cell dysfunction is a dynamic antigen-driven differentiation program initiated early during tumorigenesis. Immunity 2016;45: 389–401.
44. Thommen D, Koelzer V, Herzig P, Roller A, Trefny M, Dimeloe S, et al. A transcriptionally and functionally distinct $PD\text{-}1^+$ $CD8^+$ T cell pool with predictive potential in non-small-cell lung cancer treated with PD-1 blockade. Nat Med 2018;24:994–1004.